# Surface Features in Langmuir−Blodgett Monolayers of Predominantly Hydrophobic Poly(styrene)−Poly(ethylene oxide) Diblock Copolymer

**C. A. Devereaux and S. M. Baker***

*Department of Chemistry, Harvey Mudd College, Claremont, California 91711*

*Received July 24, 2001*

ABSTRACT: Monolayers of a predominantly hydrophobic poly(styrene)-*b*-poly(ethylene oxide) copolymer (7% PEO by mass) were transferred to a silicon substrate using the Langmuir−Blodgett method. The films were imaged using atomic force microscopy, and three types of features were observed in various proportions: dots (circular aggregates), spaghetti (rodlike aggregates), and continents (planar aggregates). The concentration of the spreading solution on the air−water interface had the most significant effect on the types of features observed. Variations in surface pressure and compression speed had little effect on the distribution and predominance of the different types of aggregates. Single-drop experiments show that feature formation depends on a competition between film spreading and polymer entanglement resulting from solvent evaporation. Aggregates thus formed upon spreading on the air−water interface are kinetically trapped and quite stable upon transfer to the solid substrate.

## 1. Introduction

Amphiphilic diblock copolymers provide a means for controlling interfacial properties or molecular architecture at various interfaces. Neutral diblock copolymers spread on an air−water interface[1] have been observed to self-assemble into nanoscale structures that have a variety of potential applications in microelectronics, stabilization, lubrication, and other fields.[2] The density of the polymer at the interface can be controlled by the choice of adsorbing block size and deposition conditions, and the properties imparted to the interface can be modified by the choice of free block. Our studies focus on poly(styrene)-*b*-poly(ethylene oxide) (PS-*b*-PEO) diblock copolymers, where we can utilize the unique aqueous surface properties of PEO and the solvent and aggregation properties of PS.

Poly(ethylene oxide) (PEO) is water-soluble and surface-active, forming monolayer films when spread on an air−water interface.[3] Above a critical surface density, a 2D critical overlap density, the PEO will submerge into the subphase; thus endcaps, such as long-chain alkanes[4] or small poly(styrene) (PS) blocks[5] are necessary to tether the PEO to the air−water interface at high surface densities. Gonçalves da Silva et al.[5] used Langmuir isotherms to determine the effective monomer area for PEO with $N_{PEO}$ between 445 and 90 and capped with $N_{PS}$ of 38. This empirical effective area was determined to be $A_{PEO} = (27\ Å^2)N_{PEO}$. The effective PEO monomer area has been observed to vary slightly with the length of the PEO chain. A later paper by Gonçalves da Silva et al.[7] reported the effective PEO monomer value to be 31 Å$^2$/monomer for PEO chains with the same PS chain length and a smaller average $N_{PEO}$. Pure PEO (with $N_{PEO}$ between 410 and 5720) has been found to have an effective monomer area of 40−48 Å$^2$/monomer,[6] suggesting a more compact structure of the tethered PEO in the diblock system than in the homopolymeric system. Our previous results for $N_{PEO} \gg 800$ and small $N_{PS}$, having a PS projected area less than the effective area of the total PEO, are consistent with 28−30 Å$^2$/monomer.[8] This selection of results suggests that PS plays only a small role in the effective PEO area in a tethered system when measured by Langmuir isotherms provided that the PS is sufficiently small.

Poly(styrene) is nonpolar and forms tightly clustered aggregates when spread at moderate concentrations under ambient conditions on an aqueous subphase. Kumaki[9] studied the properties of monomolecular PS particles by using extremely dilute spreading concentrations, on the order of $10^{-3}$ mg/mL, on a Langmuir−Blodgett trough. Judging from the isotherms he obtained, the projected area of the single PS globule is given by $0.04MW_{PS}$.[10] Given the values for projected areas of PS and PEO pancakes discussed above, the polymer blocks should have similar projected areas at 6.5% PEO (by mass).

The properties of PS-*b*-PEO at the air−water interface have been studied by a variety of techniques involving Langmuir isotherms.[4−7,11−17] When spread on an aqueous subphase, the PEO spreads, and the PS forms aggregates as a result of the repulsion between the hydrophobic PS block and the water or PEO.[18] At low surface pressures ($\pi$) defined as the difference between the surface tension of pure water and the measured surface tension ($\pi = \gamma_o - \gamma$), loose aggregates form, and the PEO chains reside at the surface of the water, spreading out in a corona around the PS cluster. At higher surface pressures, the PEO is compressed, and at 10 mN/m, a first-order 2D-to-3D phase transition occures as the PEO chains submerge into the aqueous subphase and begin to form brushes.[7,11] At surface pressures higher than 10 mN/m (lower mean molecular areas or mmA's), the PEO brushes are compressed until either the limiting PEO area or the PS limiting area is attained. For small PEO contents, the first-order phase transition of the PEO is hindered by the PS.

Our previous research[8] on predominantly hydrophilic diblock copolymers (greater than 10% PEO) suggests that the PS aggregates into uniform nanoscale dots upon spreading. Increasing the PEO content decreases the aggregation number of these circular features in a linear relationship. Additionally, the distance between features decreases with increasing deposition surface pressure, which correlates with surface density. The aggregation number does not change with increasing surface pressure, indicating that, once formed, the aggregates are stable to further aggregation.

10.1021/ma011319m CCC: $22.00 
Published on Web 01/26/2002

**Table 1. Characteristics of the 51k PS-*b*-PEO**

| MW (g/mol) | PEO wt % | polydispersity | $MW_{PEO}$ | $MW_{PS}$ | $N_{PEO}$ | $N_{PS}$ |
|---|---|---|---|---|---|---|
| 51 300 | 7.0 | 1.07 | 3600 | 47700 | 82 | 459 |

In this paper, we examine the surface morphology of a predominantly hydrophobic polymer with a smaller PEO block, 7 wt % PEO (hereafter referred to as the 51k polymer). For this asymmetry, the 2D-to-3D phase transition should be hindered by the PS block. Table 1 presents the salient features of this polymer. In addition to the influence of greater PS−PS interactions, we expect entanglement of the polymers before and during spreading to affect the morphologies observed.

Monolayer films were deposited using the Langmuir−Blodgett technique. Atomic force microscopy (AFM) was used to define the characteristics of the surface features both qualitatively and quantitatively. The surface features observed in the 51k polymer are divided into three categories: dots, spaghetti, and continents. Trends in the abundance of these features were monitored as a function of spreading solution concentration, deposition surface pressure, and compression speed. Single-drop experiments on a wafer were performed to examine the effect of drop spreading on the feature morphology.

## 2. Experimental Section

**2.1. Materials.** The 51k polymer was obtained from Polymer Labs (batch number 29170−34). High-purity (99.98%) UniSolv chloroform from Spectrum Labs was used in creating polymer solutions, and reagent grade chloroform (purity > 99.8%, also from Spectrum Labs) was used in all cleaning processes; both were used without further purification. All water was purified using the Millipore Milli-Q system (18.2 MΩ cm).

**2.2. Langmuir−Blodgett Films.** All $\pi-A$ compression isotherms (plots of surface pressure vs mean molecular area) and polymer monolayers were made with a KSV 5000 Langmuir Blodgett system (300 × 700 mm Teflon trough) installed in a Clean Air Products soft-wall clean room (CAP 577, 99.99% efficiency at 30 mm). Surface pressure measurements were made with a roughened platinum Wilhelmy plate, and the trough was cleaned to a blank surface pressure of $\pi < 0.15$ mN/m before each trial. Silicon substrates from Silicon Quest International (resistivity of 0.01−0.02 Ω cm, 2-in. in diameter) were sonicated in high-grade chloroform for 20 min and subsequently ozonated for 15 min in a Jelight UVO cleaner, model 42.

Solutions of the 51k polymer in chloroform were spread on the clean trough surface using a Hamilton gastight microliter syringe. In the surface pressure and compression speed trials, solutions with a concentration of 1.00 ± 0.07 mg/mL were used, whereas the concentration was varied as noted in the concentration trials. The amount of polymer spread in each trial was calculated from values obtained from the $\pi-A$ isotherm and ranged from 25 to 850 μL. The solution was added dropwise to the water subphase at uniformly spaced locations across the surface until the syringe was emptied. The solvent was then allowed to evaporate from the trough for 15 min.

Films were depositied at pressures corresponding to areas larger than the critical PEO density at the surface, which were between 0.3 and 10 mN/m. Compression to the desired surface pressure was carried out at a speed of 60 $cm^2$/min (10 mm/min for a standard 300 × 700 mm trough) for the pressure and concentration trials and at variable speeds for the compression speed trials. Once the desired surface pressure was achieved, the system was allowed to equilibrate for 10 min. The submerged substrate was then withdrawn from the water at a speed of 0.5 mm/min and allowed to dry for at least 15 h in the clean room.

**2.3. AFM Imaging.** A Dimension 3000 atomic force microscope in tapping mode was used for all imaging (tip length, 125 μm; frequency, 279−362 kHz; Digital Instruments). The AFM was housed in a vibration-resistant case. Each sample was imaged in air at a variety of locations on the wafer to examine the reproducibility of the features observed in the images. The scan speed was typically 2.5 Hz. Images shown were plane-fitted, and in a few cases flattened, to maximize image presentability. Measurements of height, width, and spacing were taken from sectional analyses of the images. All images are 4 μm on a side, with heights and gray scales chosen to optimize presentability. Actual heights are presented in Table 2. A total of 288 images were collected, excluding the single-drop experiments, described in section 3.4.

## 3. Results and Discussion

**3.1. Isotherm.** The $\pi-A$ isotherm shown in Figure 1 for the 51k polymer displays no plateau at 10 mN/m, unlike the isotherms of more hydrophilic copolymers[8] and consistent with the overlap of PS before the PEO phase transition. The features of the isotherm are independent of compression speed and concentration. Fauré et al.[14] observed a similar absence of a plateau when the PS block was relatively large or the PEO was very small, regardless of PS block size. The homopolymer of PS at the air−water interface has a fairly featureless isotherm with a collapse near 60 mN/m.[19] Using the reported monomer area values for the morphological transitions of PEO aggregates,[20] the 51k polymer is expected to reach the limiting pancake at 2214 $Å^2$ and the 2D-to-3D phase transition at 1640 $Å^2$. The latter corresponds to the pancake-to-brush transition at approximately 10 mN/m in the isotherm data of Figure 1. All Langmuir−Blodgett films presented here were deposited at values at or below this surface pressure to ensure a nominally 2D PEO layer.

**3.2. Variation of Parameters.** Three types of features (dots, spaghetti, and continents) were observed in various proportions in the AFM images. Figure 2 demonstrates the range of features observed. In all AFM images, lighter shading in the image indicates higher features. Most images are from the surface pressure trials, where the concentration was 1 mg/mL, the compression speed was 60 $cm^2$/min, and the films were deposited at various surface pressures. Images were randomly chosen to highlight the range of observed features. It is important to note that, although trends were observed in the predominance of certain features, no substrate had only one feature present. In all of the samples observed, the three types of features were either intermingled or observed at various regions of the surface independently. However, certain deposition conditions affected the predominant feature type observed. Three of the deposition conditions were varied in an effort to favor the formation of certain features.

Figure 3 shows the variety of sizes and shapes of the predominant features. In row 1, samples of the continents observed are shown with various widths, with no size correlation observed for the parameters varied. The sizes of the dots, shown in row 2, vary significantly depending on the location on the surface, with examples of larger to smaller dots shown from A to D. However, these sizes do not follow any trend in terms of parameter variations either. Interestingly, the spaghetti, with examples shown in row 3, is observed to be of a fairly consistent width and height, whether found alone in a particular area, extending from continents, or weaving through dots. Additionally, the spaghetti is very flexible and thin enough to withstand 180° turn without break-

**Table 2. Average Sizes of Observed Features**[a]

| | compression speed trials | | | concentration trials | | | surface pressure trials | | |
|---|---|---|---|---|---|---|---|---|---|
| | dots | spaghetti | continents | dots | spaghetti | continents | dots | spaghetti | continents |
| height | 6.8 (1.1) | 7.3 (1.0) | 5.2 (1.0) | 6.8 (1.1) | 6.9 (0.7) | 4.8 (0.8) | 6.9 (1.0) | 7.0 (0.8) | 5.0 (0.8) |
| width | 100 (49) | 97 (39) | 624 (690) | 103 (52) | 192 (18) | 717 (720) | 105 (45) | 96 (25) | 620 (670) |
| no. of samples | 49 | 54 | 40 | 39 | 52 | 63 | 52 | 68 | 43 |

[a] Values are in nanometers; standard deviations are in parentheses.

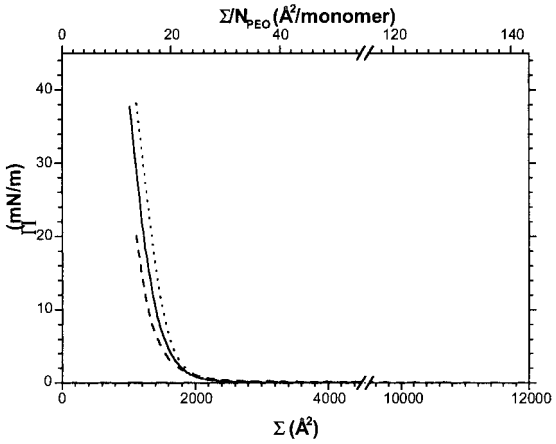


**Figure 1.** Langmuir isotherm for the 51k polymer. Σ is the mean molecular area, and $\Sigma/N_{PEO}$ is the mean molecular area per PEO monomer. $\pi$ is the surface pressure determined by Wilhelmy plate measurements. No plateau is observed because of the presence of a large PS block. Isotherms are shown for three different runs to demonstrate reproducibility.

ing. The continents break with very sharp, straight cracks. The extra mass at the end of the crack under compression can be seen in the AFM images.

To quantify the features observed as a function of compression speed, concentration and deposition pressure, all images were analyzed, and the data are presented in terms of "average % feature" values. In the following plots, the average % feature value was determined as follows: For each of the ∼300 images, an assessment of the fractional area covered by each type of feature, dots, spaghetti, or continents, was recorded. In some cases, no error was observed because the image contained exclusively one feature type. In the worst case, when there were two or three feature types present, the percent coverage could be determined to within the square of the spacing between features, typically on the order of $(100\ nm)^2$, divided by the total area of the image, most being $(4\ \mu m)^2$. For a worst-case assessment of 500-nm spacing, the error is less than 2%. The difficulty becomes one of assignment of feature type in crossover structures. For each point on the plots shown in Figures 4−6 described below, the percentages for all images fitting the given conditions were averaged. Thus, these average percentages represent the feature distribution for each set of conditions.

*Compression Speed.* The compression speed is a measure of how quickly the trough barriers reduce the area occupied by the spread and evaporated polymer film. In these trials, the compression speed was varied from 3 to 600 $cm^2$/min (from 0.5 to 100 mm/min) while the concentration held at 1 mg/mL and the surface pressure at 2 mN/m. The results are plotted in Figure 4. No particular trend in feature predominance is associated with compression speed. Fluctuations are probably due to the statistical distribution of features over the entire sample and our sampling size. It is worthwhile to note that, for almost all compression speed trials, dots were the predominant feature observed.

*Deposition Pressure.* Surface pressure ($\pi$) correlates with a particular mmA, as reflected by the isotherm, and was maintained at a given value for the duration of the film deposition onto the substrate. For this comparison, $\pi$ was varied from 0.3 to 10 mN/m, with the compression speed maintained at 60 $cm^2$/min and the concentration at 1 mg/mL. The mean molecular area (Σ) varies from 24 to 17 $Å^2$/monomer, which is below the critical PEO surface density. As with the compression speed trials, no clear trend in predominant feature was observed for varying surface pressure (see Figure 5). This observation is consistent with our theory that the features are formed immediately after deposition as the solvent evaporates.[8] By the time the solvent has evaporated, the features have already formed and are kinetically trapped. Once formed, the features do not break up or aggregate further upon compression by the barriers.

Increasing surface pressure of the deposition, however, decreased the spacing, as observed previously,[8] but only slightly. Over the range of pressures used, the variation in mmA was <30%. As this region of the isotherm is so steep, the spacing changes only slightly in the range of pressures studied. Again, dots were observed as the predominant feature.

*Spreading Solution Concentration.* The concentration of the polymer in chloroform was varied from 0.1 to 4 mg/mL for a series of depositions where the compression speed was held constant at 60 $cm^2$/min and the surface pressure was held at 2 mN/m. Dots were favored at lower concentrations, and continents were favored at higher concentrations (see Figure 6). Note that, in the previous two trials, although other parameters were varied, the concentration was held at 1 mg/mL, and dots were predominant.

In Figure 6, a point of inversion in the predominant feature observed exists near 1.6 mg/mL, indicating the change in preferable formation from dots to continents. The critical overlap concentration ($c^*$) cannot explain the dramatic inversion point observed near 1.6 mg/mL. The radius of gyration ($R_g$) is related to the critical overlap concentration by the equation $c^* = (3MW)/(4\pi N_A\langle R_g^2\rangle^{3/2})$, where MW is the molecular weight of the entire polymer and $N_A$ is Avogadro's number. The radius of gyration of a polymer chain in a good solvent is that for the Flory radius, $\langle R_g^2\rangle^{1/2} = aN^{0.6}$, where $a$ is the effective monomer length and $N$ is the number of PS units in the polymer (here, $N$ is 459 for PS). A consistent value measured for $a$ is 1.8 Å, as determined by light-scattering experiments for PS in toluene.[21−23] Given this value, $c^*$ for the 51k polymer is greater than 50 mg/mL. Even though our polymer is dissolved in chloroform, the $c^*$ value is likely not an order of magnitude smaller. Clearly, another mechanism is responsible for the inversion of features.

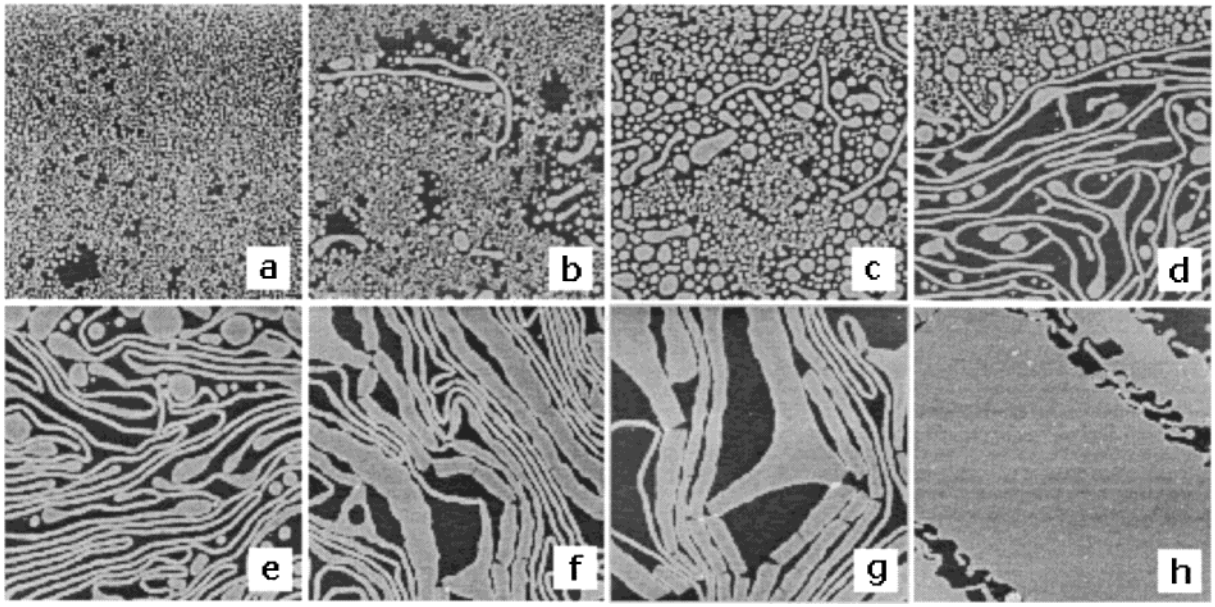


**Figure 2.** Sample AFM images (4 $\mu$m × 4 $\mu$m, heights discussed in Table 2) of the types of features observed. All samples are from a 1 mg/mL spreading solution and all but g were compressed at 60 cm$^2$/min (g was compressed at 240 cm$^2$/min). Images a−c are mostly dots, d−f are mostly spaghetti, and g−h are mostly continents. $\pi$ (mN/m) = (a) 2, (b) 0.5, (c) 0.3, (d) 2, (e) 6, (f) 4, (g) 2, (h) 10.

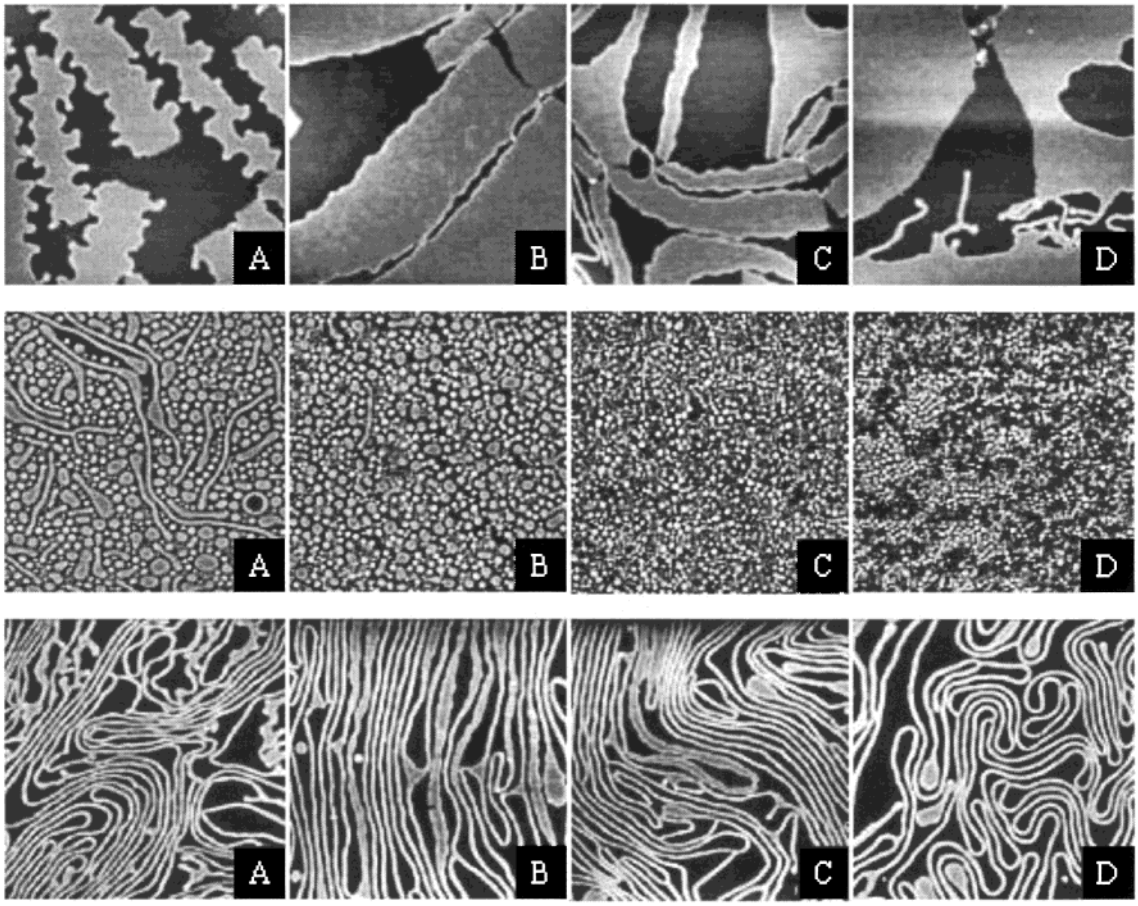


**Figure 3.** Sample AFM images (4 $\mu$m × 4 $\mu$m, heights discussed in Table 2) of the specific features observed. Row 1, continents; row 2, dots; row 3, spaghetti. The deposition variables for each image are $\pi$ = 2 mN/m, concentration = 1 mg/mL, and compression speed = 10 mm/min except as follows: (1A) concentration = 1.7 mg/mL, (1B) concentration = 3.5 mg/mL, (1D) concentration = 1.7 mg/mL, (2A) $\pi$ = 1 mN/m, (2B) $\pi$ = 4 mN/m, (2C) compression speed = 20 mm/min, (2D) $\pi$ = 4 mN/m, (3B) $\pi$ = 0.5 mN/m, (3C) $\pi$ = 6mN/m, and (3D) concentration = 0.5 mg/mL.

The obvious point of inversion in Figure 6 suggests that the degree of polymer overlap as the solution spreads plays a major role in the types of features created. Kumaki[10] found that pure PS spread from benzene starts to aggregate at concentrations of 2 × $10^{-3}$ mg/mL and higher but that, below that concentra-

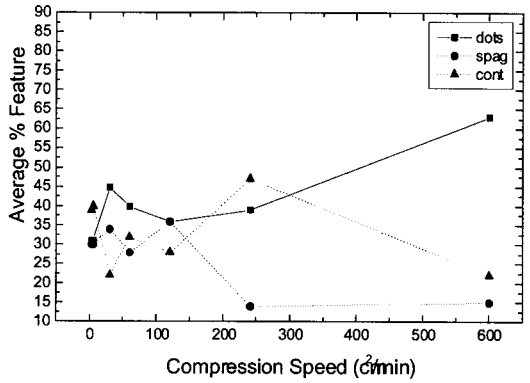


**Figure 4.** Plot of frequencies with which the three types of features were observed with varied compression speed ($\pi = 2$ mN/m and concentration = 1 mg/mL). Total number of images = 288.

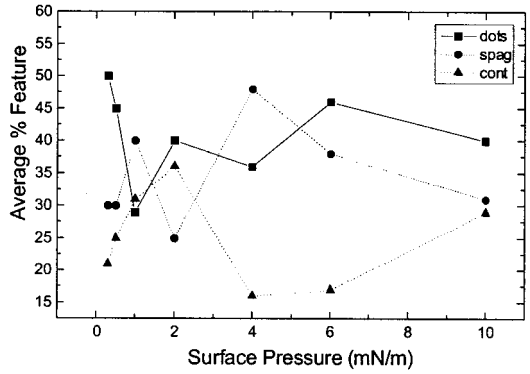


**Figure 5.** Plot of frequencies with which the three features were observed with varied surface pressure (compression speed = 60 cm$^2$/min and concentration = 1 mg/mL). Total number of images = 288.

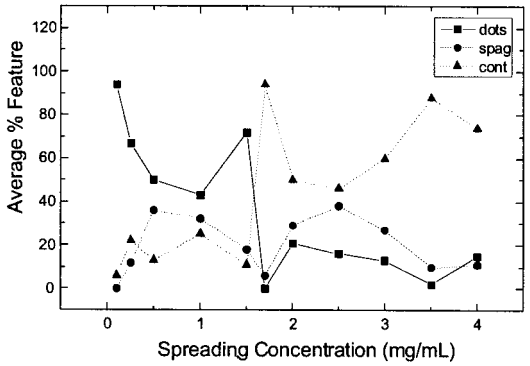


**Figure 6.** Plot of frequencies with which the three features were observed with varied deposition concentration ($\pi = 2$ mN/m and compression speed = 60 cm$^2$/min). Total number of images = 288.

tion, individual PS particles could be isolated. In the case of the PS-*b*-PEO diblock, the PEO spreading can compete with aggregation. Aggregation is always observed at the concentrations used in these experiments (>0.1 mg/mL); however, the effective aggregate number is a function of the concentration.

**3.3. Characteristics of Features.** Table 2 presents a summary of the dimensions of the features observed in the majority of the 288 AFM images taken as a comparison between the various trails. Some of the images having mixed features that were difficult to assess independently were not used. The analyses were done as follows. To be classified as a dot, the feature must be less than 300 nm in diameter in any direction and have an aspect ratio of 3:1 or less. These criteria categorize dots as small conglomerates that are roughly circular. Dots are observed to have a wide range of diameters, ranging from 70 to 250 nm. Spaghetti are features that have at least one cross-sectional width less than 150 nm if their aspect ratio is between 3:1 and 10:1 and less than 200 nm at all times, even for aspect ratios of greater than 10:1. These criteria ensure a long, stringy appearance. Most spaghetti formations are seen in the range of 70−130 nm thick. Finally, if a feature is too large to be contained in the above criteria, it is considered a continent. A tremendous variation in size is observed, with the larger continents being several microns wide. If a continent contains characteristics of another feature connected to it, most notably spaghetti, the feature is still considered part of the continent.

Table 2 shows that, overall, dots and spaghetti were ∼6−7 nm tall and 70−100 nm wide. Continents tended to be shorter (∼5 nm) and wider (>200 nm) and to exhibit the largest statistical variation in size, as small as the dot-limiting definition and as large as an entire 6-$\mu$m AFM image. The spacing between features was much more variable than the feature dimensions and likely reflects the spreading of the drops as explored in section 3.4.

A comparison between the measured film thickness for a variety of features and the height of independent PS homopolymer globules can provide information about the packing of the aggregates in these features. The feature heights concur that the film is a monolayer in thickness with minimal distortion relative to a "free" PS globule. Using Kumaki's value for PS area[10] and assuming a spherical PS particle, the expected diameter of a single collapsed random PS coil of the 51k polymer in air is 5.0 nm. The height of the continents is generally smaller than those of the dots and spaghetti, indicating that the PS in the continent features is laterally entangled and not compressed significantly, an effect that would cause the continents to be more brushlike and taller. However, the lateral features are between 50 and several thousand times wider than a single molecule, a value that indicates that the extent of overlap is tremendous. The slightly taller dots and spaghetti may reflect the minimization of the surface free energy of the PS. This motion is more restricted in the much wider continents, although we see evidence of a 1−2-nm "rim" on all of the features wider than ∼150 nm.

Whereas the type of feature predominantly observed in our studies appears to be related to the spreading solution concentration, Zhu et al.[24,25] found that changing the percentage of PS in poly(styrene)−4-vinyl pryidinium decyl iodide (P4VP) copolymer solutions affected the types of features seen. Specifically, 6% PVP and lower gave planar aggregates, 6−14% PVP gave rods, and 14% PVP and higher gave starfish micelles. Our interesting result is that the three features can be observed from a single polymer asymmetry as a function of spreading solution concentration.

Similar 3D morphologies have also been observed in water−THF solutions of PS-*b*-PEO. Yu et al.[26,27] created micelles in solution by adding water to solutions of polymers in THF until aggregates formed. They observed "tubules" (rodlike micelles) when they used a 2.6% PEO polymer at 1.5 or 2.0 wt % (15 or 20 mg/mL). They also observed aggregates similar to our continents when using a 7.3% PEO polymer at a concentration of

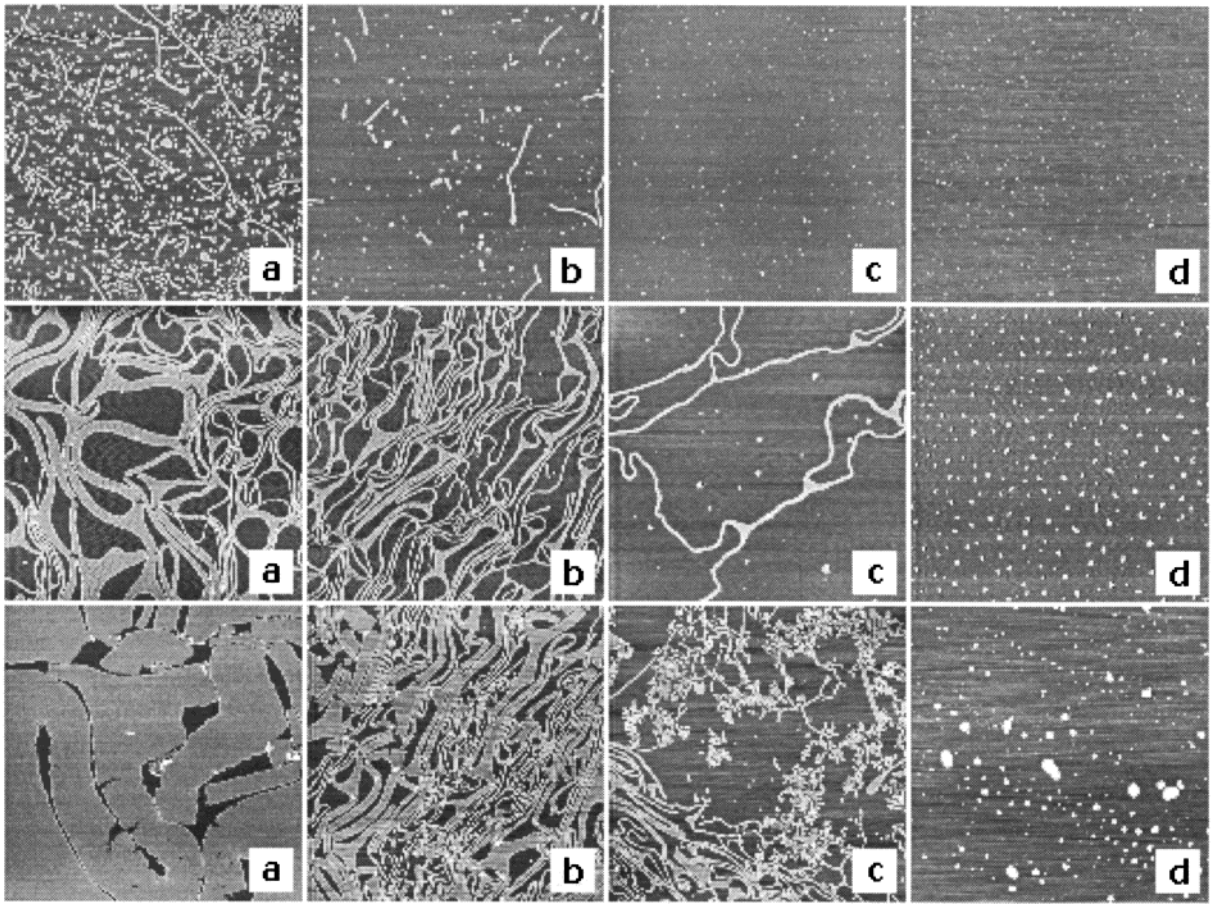


**Figure 7.** Spaghetti-rich AFM image (concentrated = 1 mg/mL, $\pi$ = 2 mN/m, compression speed = 120 cm$^2$/min) and its cross section, demonstrating the uniform spacing between features. The images are each 4 $\mu$m × 4 $\mu$m, have a height scale of 50 nm, and progress from the center of the water (a) outward (b−d).

1.5 wt % (15 mg/mL). Although these "lamellae" formed at higher concenration appear comparable to our continents, they are more than 6 times thicker than our aggregates. The analogy to the 3D system is intriguing, but the 3D system is more likely an equilibrium state rather than the result of a trapped kinetic state.

**3.4. Single-Drop Experiments.** To study the interplay between solvent evaporation and polymer entanglement, a supplementary experiment was undertaken to mimic the conditions of a single drop spread during the application of the polymer to the Langmuir−Blodgett trough. In this experiment, a drop of polymer solution was applied to the center of a wetted silicon substrate. The aqueous layer on the substrate was ∼0. 5 mm tall. The substrate was allowed to dry in the clean room for 1 week and was then imaged by AFM. The morphologies of a single drop spread at the air−water interface could be examined without some of the potential complications of transfer from the aqueous to solid substrate. However, for low-concentration drops, the lack of film continuity caused some clumping of the drying thin films. Because surface pressure and compression speed were found to be negligible, only concentration was varied. This single-drop experiment was done at concentrations below, above, and near the feature inversion point (∼1.6 mg/mL).

The first row in Figure 7 shows a progression of images from the 1 mg/mL trial. This concentration was less than the observed inversion concentration, $c_{inv}$, as suggested by Figure 6, and sparse dots were observed over most of the wafer. Spaghetti was present only at the very interior of the wafer, and continents were not observed at all. This distribution of features is consistent with an even spreading of the polymer across the wafer. It is important to note that, in the two trials below $c_{inv}$, the film was not as cohesive as in the higher-concentration trials. Portions of the film tended to move with the water subphase as it evaporated, leading to patches of obviously anomalous features. As no long-range interactions across the film existed to provide cohesive strength laterally, the film broke and followed the evaporation front of the water.

When a polymer concentration near the feature inversion point was used (1.5 mg/mL), spaghetti and thin continents were observed from the center to almost the edge of the wafer, with tall (∼100 nm) dots at the very edges. As can be seen in the second row of Figure 7, a slight size change in the width of continents was observed in the direction radially outward from the center of the wafer. At approximately 30 mm from the center and farther, large dots were observed. Interestingly, the predominance of spaghetti in this experiment was much higher than in the trials carried out on the Langmuir−Blodgett trough.

The third row of Figure 7 shows the progression of features observed in the high-concentration trial (5 mg/mL). Continents were observed up to approximately 35 mm from the center of the wafer. Near the center of the wafer, the continents covered the surface almost entirely, with only small holes breaking the large expanses of film. Radially farther out, these continents became smaller and farther apart. Between 35 and 40 mm (with

the edge of the wafer at ca. 40 mm), spaghetti and large dots were observed. The feature progression was similar to that in the 1.5 mg/mL trial, with continents near the center, then spaghetti, and then dots at the edges of the wafer.

The data for concentrations above and near the feature inversion point suggest that the different features formed on the trough are due to competition between solvent evaporation and entanglement. As the droplet spreads, the solvent evaporates. Polymers at the leading edge of the spreading drop have the highest solvation. As the solvent evaporates, the features toward the center of the drop experience a higher concentration and become more entangled. Continents form on the interior of the wafer because the polymers cannot spread before the solvent evaporates. Additionally, the correspondence in features between the single-drop experiment and the Langmuir−Blodgett samples suggests that the features observed via AFM are indeed the features formed on the trough's aqueous surface and that the spread drop structure is maintained upon compression.

This interplay between solvent evaporation and entanglement indeed produces interesting effects. To gain further understanding of the spreading phenomena, we plan on using solvents with different vapor pressures to vary the evaporation rate and thus affect the aggregation of the copolymers upon spreading. By controlling the evaporation rate versus the spreading rate, we hope to isolate certain features as has been done for mixed systems of 3D aggregates.[28] We will also vary the temperature to change the evaporation rate on the Langmuir trough, a measurement that will also allow us to determine enthalpic and entropic information about the compression.

## 4. Conclusions

In the current study, surface pressure and compression speed were observed to have minimal effects on the type of features observed. This result indicates that isotherms and depositions can be run relatively quickly and still yield reliable, reproducible results. The predominant feature observed is a result of the spreading solution concentration, and an inversion concentration is observed for this polymer at 1.6 mg/mL in chloroform. Consequently, the judicious choice of spreading solution concentration allows for selection of the predominant surface feature. Finally, the morphologies observed reflect a distribution of features that result from the droplet spreading on a surface. Although the predominant feature produced can be controlled by the choice of concentration, all types of features—dots, spaghetti, and continents—are observed on substrates prepared both from Langmuir−Blodgett deposition and from single-drop experiments on a wafer.

Using the results from both past and present research, we have developed a large degree of control over the predominant types of molecular architectures formed by diblock copolymers. For PS-*b*-PEO with greater than 10% PEO, we observe only dots and can control feature spacing via deposition pressure and feature size by selection of the appropriate total molecular weight and PEO content.[8] Conversely, for copolymers with less than ∼7% PEO, we can favor the formation of certain types of features by the choice of spreading concentration. This research demonstrates the large extent to which polymer entanglement plays a role in the types of features observed in self-assembled diblock copolymer films and reveals how rational selection of deposition and spreading solution parameters allows further control of polymer morphology.

**Acknowledgment.** This material is based on work supported by the National Science Foundation under Grant 9623718 and the Research Experiences for Undergraduates program. Part of this work was supported by the Department of Energy through a PECASE award. The authors thank Aaron Jacobs for his diligence in the statistical analyses of many samples.

## References and Notes

(1) Li, S.; Hanley, S.; Khan, I.; Varshney, S. K.; Eisenberg, A.; Lennox, R. B. *Langmuir* **1993**, *9*, 2243−2246.
(2) Koutsos, V.; van der Vegte, E. W.; Pelletier, E.; Stamouli, A.; Hadziioannou, G. *Macromolecules* **1997**, *30*, 4719−4726.
(3) Kuzmenka, D. J.; Granick, S. *Macromolecules* **1988**, *21*, 779−782.
(4) Barentin, C.; Muller, P.; Joanny, J. F. *Macromolecules* **1998**, *31*, 2198−2211.
(5) Gonçalves da Silva, A. M.; Filipe, E. J. M.; d'Olivera, J. M. R.; Martinho, J. M. G. *Langmuir* **1996**, *12*, 6547−6553.
(6) Sauer, B. B.; Yu, H. *Macromolecules* **1989**, *22*, 786−791.
(7) Gonçalves da Silva, A. M.; Simoes Gamboa, A. L.; Martinho, J. M. G. *Langmuir* **1998**, *14*, 5327−5330.
(8) Baker, S. M.; Leach, K. A.; Devereaux, C. A.; Gragson, D. E. *Macromolecules* **2000**, *33*, 5432−5436.
(9) Kumaki, J. *Macromolecules* **1986**, *19*, 2258−2263.
(10) Kumaki, J. *Macromolecules* **1988**, *21*, 749−755.
(11) Bijsterbosch, H. D.; de Haan, V. O.; de Graaf, A. W.; Mellma, M.; Leermakers, F. A. M.; Cohen Stuart, M. A.; van Well, A. A. *Langmuir* **1995**, *11*, 4467−4473.
(12) Charron, J. R.; Tilton, R. D. *Langmuir* **1997**, *13*, 5524−5527.
(13) Dewhurst, P. F.; Lovell, M. R.; Jones, J. L.; Richards, R. W.; Webster, J. R. P. *Macromolecules* **1998**, *31*, 7851−7864.
(14) Fauré, M. C.; Bassereau, P.; Carignano, M. A.; Szleifer, I.; Gallo, Y.; Andelman, D. *Eur. Phys. J. B* **1998**, *3*, 365−375.
(15) Fauré, M. C.; Bassereau, P.; Lee, L. T.; Menelle, A.; Lheveder, C. *Macromolecules* **1999**, *32*, 8538−8550.
(16) Sauer, B. B.; Yu, H.; Tien, C.; Hager, D. F. *Macromolecules* **1987**, *20*, 393−400.
(17) Gragson, D. E.; Jenson, J.; Baker, S. M. *Langmuir* **1999**, *15* (19), 6127−6131.
(18) Zhu, J.; Eisenberg, A.; Lennox, R. B. *J. Am. Chem. Soc.* **1991**, *113*, 5583−5588.
(19) Faure, M. C.; Bassereau, P.; Carignano, M. A.; Szleifer, I.; Gallo, Y.; Andelman, D. *Eur. Phys. J. B* **1998**, *3*, 365−375.
(20) Kumaki, J. *Macromolecules* **1988**, *21*, 749−755.
(21) Limiting pancake area of 27 Å$^2$/monomer and 2D-to-3D transition at 20 Å$^2$/monomer as reported in ref 5.
(22) Corrotto, J.; Ortega, F.; Vàszquez, M.; Freire, J. J. *Macromolecules* **1996**, *29*, 5948−5954.
(23) Szydlowski, J.; Van Hook, W. A. *Macromolecules* **1998**, *31*, 3266−3274.
(24) Higo, Y.; Ueno, N.; Noda, I. *Polym. J.* **1983**, *15*, 367.
(25) Zhu, J.; Lennox, R. B.; Eisenberg, A. *J. Phys. Chem.* **1992**, *96*, 4727−4730.
(26) Zhu, J.; Eisenberg, A.; Lennox, R. B. *Macromolecules* **1992**, *25*, 6547−6555.
(27) Yu, K.; Zhang, L.; Eisenberg, A. *Langmuir* **1996**, *12*, 5980−5984.
(28) Yu, K.; Eisenberg, A. *Macromolecules* **1998**, *31*, 3509−3518.
(29) Yu, Y.; Eisenberg, A. *J. Am. Chem. Soc.* **1997**, *119*, 8383−8384.

MA011319M